Redefining kiss-and-run and full-collapse fusion for dense-core vesicles: structural changes, triggers, and pivotal endocytic roles

Hsueh-Cheng Chiang[*1], Wonchul Shin[*1], Wei-Dong Zhao[1], Edaeni Hamid[1], Jiansong Sheng[1], Maryna Baydyuk[1], Peter J. Wen[1], Albert Jin[2], Fanny Momboisse[ξ1], and Ling-Gang Wu[1]

1. National Institute of Neurological Disorders and Stroke, 35 Convent Dr., Bldg 35, Rm. 2B-1012, Bethesda, Maryland 208922.
2. National Institute of Biomedical Imaging and Bioengineering (NIBIB), Bethesda, MD 20892

*: equal contribution

ξ: Current address: Neuroscience Center, University of Valparaíso, Gran Bretaña 1111, Playa Ancha, Valparaíso, Chile

Supplementary Materials

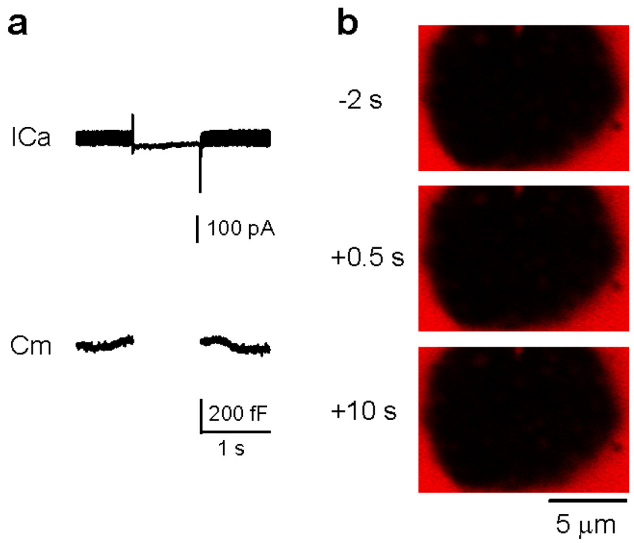

Figure S1. Depolarization induced no capacitance jump or fluorescence spot in the absence of the extracellular calcium

(**a-b**) ICa (a, upper), Cm (a, lower) and A647 image (b) induced by a 1 s depolarization (-80 to +10 mV) in a bath solution containing 0 mM calcium, 2 mM EGTA, and 30 μM A647. In panel b, cell-bottom images were taken at 2 s before (upper), 0.5 s during (middle), and 10 s after (lower) the 1 s depolarization.

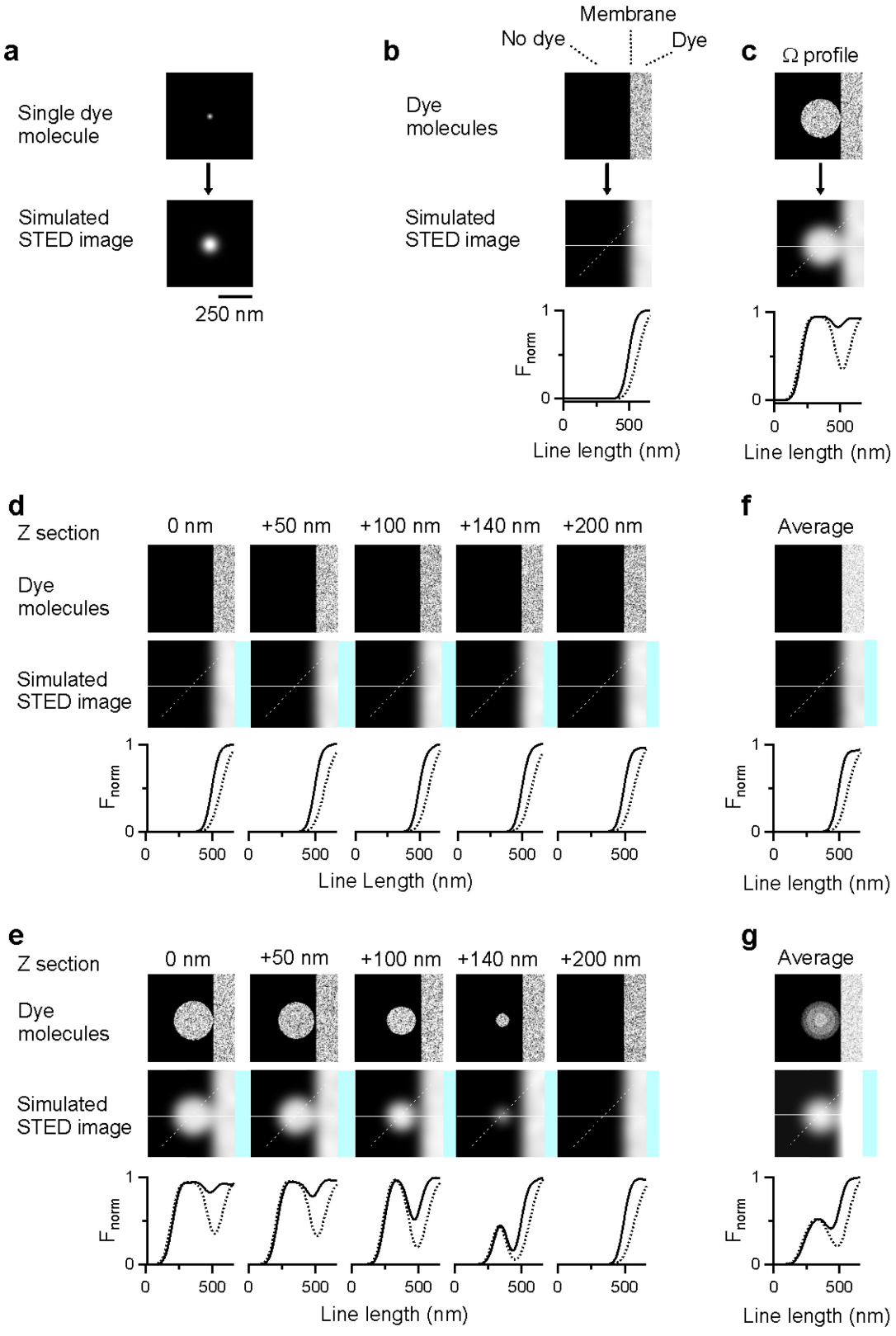
a
Single dye molecule
Simulated STED image
250 nm
b
Membrane
No dye
Dye
Dye molecules
Simulated STED image
F norm
1
0
0
500
Line length (nm)
c
Ω profile
1
0
0
500
Line length (nm)
d
Z section
0 nm
+50 nm
+100 nm
+140 nm
+200 nm
Dye molecules
Simulated STED image
F norm
1
0
0
500
Line Length (nm)
f
Average
F norm
1
0
0
500
Line length (nm)
e
Z section
0 nm
+50 nm
+100 nm
+140 nm
+200 nm
Dye molecules
Simulated STED image
F norm
1
0
0
500
Line length (nm)
g
Average
F norm
1
0
0
500
Line length (nm)

Figure S2

Figure S2. Simulated side image of an Ω-profile at the fusion instant and its line profiles

(**a**) **Two-dimension (2-D) simulation of a point light source**

A single fluorescent molecule (point source, upper) is converted to a simulated STED image (lower) using a Gaussian function with a half width of 100 nm at a 2-D plane.

(**b**) **Two-dimension simulation of a resting membrane**

Upper: a resting membrane at 2-D plane with A647 molecules (dye, bright) in the right, but not in the left side (black).

Middle: assigning each A647 molecule in the upper panel with a simulated STED image as in panel a yields a simulated STED image of the upper panel.

Lower: the fluorescence intensity profiles of two equal-length lines, one horizontal (solid), the other 45^o apart (dotted, see also panel c for defining these two lines).

(**c**) **Two dimension simulation of a Ω-profile at the instant of fusion**

Similar arrangements as panel b, except that a Ω-profile (diameter: 300 nm, pore: 50 nm) is attached at the membrane. The Ω-profile is filled with A647 molecules.

The Ω-profile is produced from a round sphere with a diameter of 300 nm, which is cut such that the diameter of the cut plane is 50 nm. The figure shows only the 2-D plane across the center of the round sphere in the z dimension.

Two equal-distance lines are drawn across the center of the sphere, one perpendicular to the membrane (solid), the other 45^o apart (dotted). Two lines cross at the center of each line.

(**d**) **Two-dimension simulation of a resting membrane at various z-sections**

Similar arrangements as in panel b, but with various z-planes as labeled.

(**e**) **Two-dimension simulation of a Ω-profile at various z-sections**

Similar arrangements as in panel c, but with various z-planes as labeled (0 nm means the horizontal section at the center, the same as panel c).

(**f-g**) **Three-dimension simulation of a resting membrane (f) and a Ω-profile (g)**

The upper and middle images in panels f and g are averaged images from all images in the upper and middle rows in panels d and e, respectively. The line profiles (lower) were obtained from the averaged image in the middle panel.

Since the z resolution of our STED or confocal microscope was ~700 nm, the dye fluorescence in a 300 nm vesicle would all be collected in the STED imaging. We therefore approximate a STED image as the average of all 2-D images, including those above and below the vesicle, but within 350 nm from the center of the 300 nm vesicle. For simplicity, we averaged only a few 2-D images shown in panels d and e. However, a similar Ω-profile and line profiles were observed if we took as many as 30 2-D images (not shown).

Conclusion: The Ω-profile can be identified by visual examination of side image and its line profiles (panel g: a dip of both lines with a larger and wider dip for the 45^o line).

Methods: Simulation was performed in IGOR software with custom-made program.

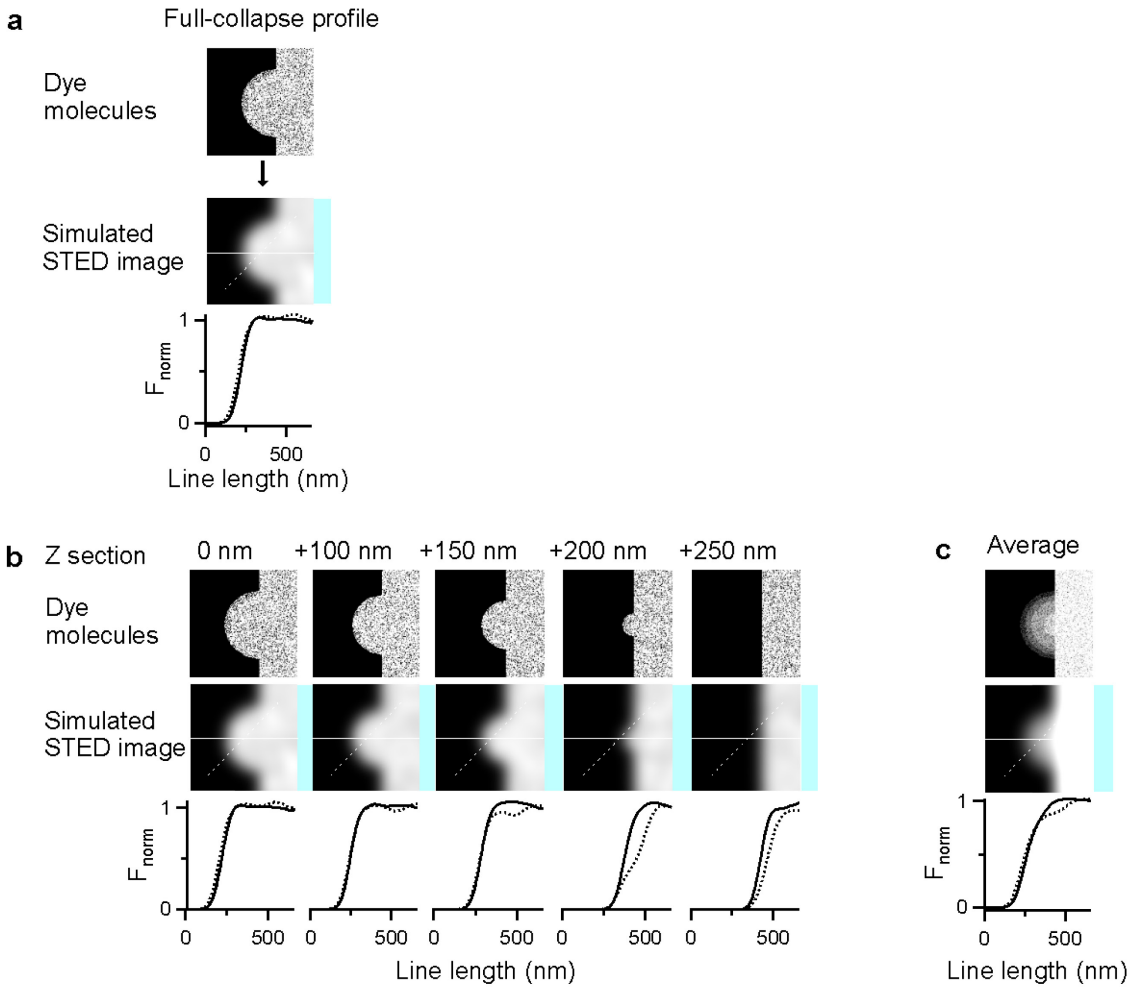

Figure S3. Simulated side image of the presumed full-collapse fusion and its line profiles

(**a**) **Two-dimension simulation of a presumed full-collapse profile**

Arrangements are similar to Fig. S2c, except that the Ω-profile is replaced with a half-sphere with a diameter of 424 nm to mimic a presumed full-collapse profile. We set the diameter as 424 nm, because the surface area of the half-sphere is the same as a sphere with a diameter of 300 nm (mean granule diameter).

(**b**) **Two-dimension simulation of a presumed full-collapse profile at various z-sections**

Similar to panel a, but at various z-planes as labeled (0 nm represents the z section across the center of the half sphere, the same as in panel a).

(**c**) **Three-dimension simulation of a presumed full-collapse profile**

The upper and middle images were the averages from images in upper and middle rows in panel b, respectively. Line profiles (lower) in the middle image are also shown.

Conclusion: The full-collapse-like profile can be distinguished by visual examination of the image and their line profiles (panel c: no dips).

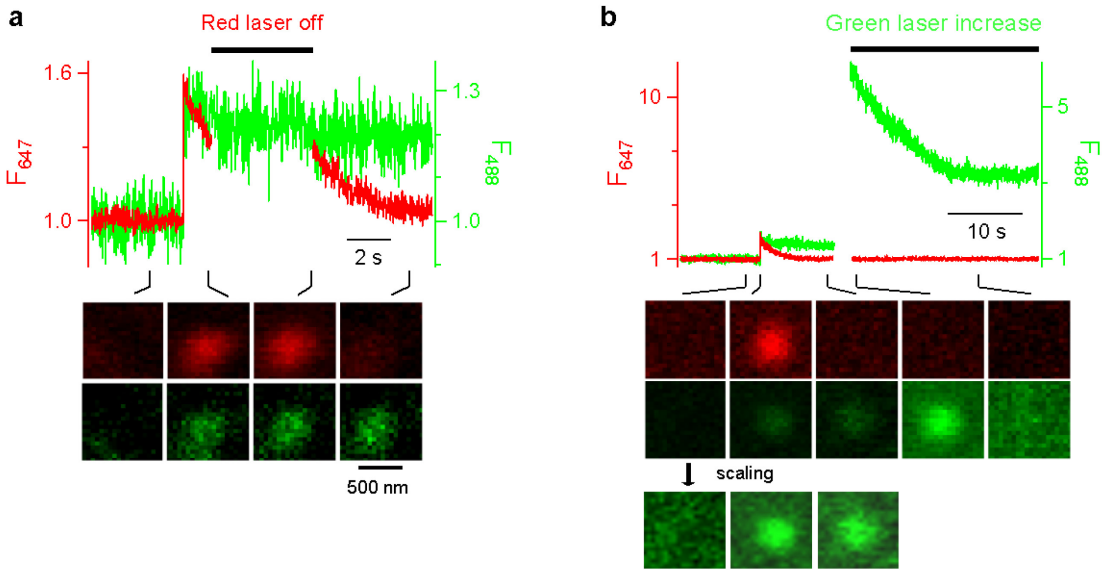

Figure S4. Strong excitation decreases F_{647} or F_{488} after fusion pore closure

(**a**) Upper: F_{647} (left) and F_{488} (right) of a spot undergoing Ω-close fusion at the confocal/cell-bottom/A647/A488 setting (strong excitation for A647, weak excitation for A488; 30 μM A647 and 30 μM A488 in the bath). At the middle of the F_{647} decay, A647 excitation was reduced to 0 for ~5 s (bar), and then resumed to the original level. Upon resuming excitation, F_{647} also resumed to the previous level and then continued to decay exponentially to the baseline, indicating that F_{647} decay is due to dye bleaching by strong excitation (after pore closure).

Lower: Sampled A647 and A488 images at times indicated (lines).

(**b**) Upper: F_{647} (left) and F_{488} (right) of a spot undergoing Ω-close fusion. In the first 20 s, the setting was the regular confocal/cell-bottom/A647/A488 setting (strong excitation for A647, weak excitation for A488). F_{647} decayed to the baseline while F_{488} remained unchanged, indicating pore closure. About 2 s later, the excitation intensity for A488 was significantly increased (bar), leading to an increase of F_{488}, followed by an exponential decay to a new baseline, at which the fluorescent spot was bleached (see image below).

Lower: Sampled A647 and A488 images at times indicated (lines). Left three A488 images obtained at weak excitation were too dim to see clearly when they were plotted at the same scale with those obtained at strong excitation. They were re-scaled to see more clearly (lowest three images).

Conclusion: strong excitation bleaches the fluorescence spot (after pore closure).

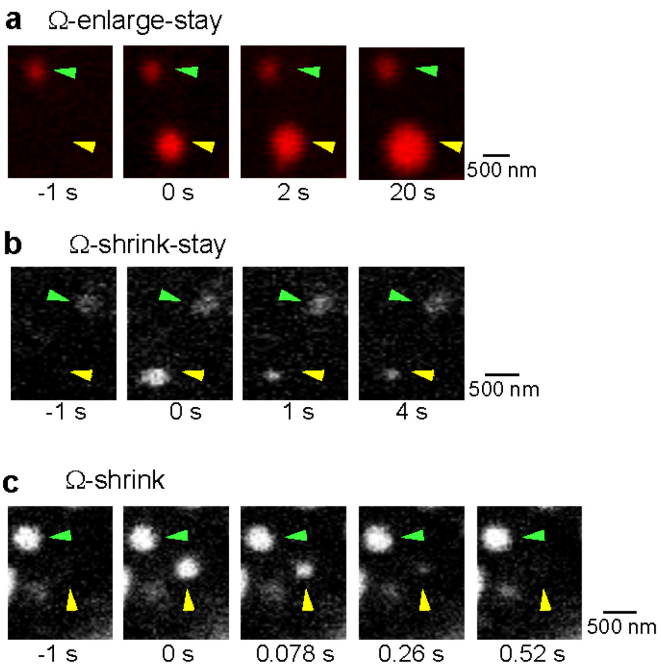

Figure S5. The enlargement or the shrinkage of the fluorescent spot is not due to focal plane changes

(a) A647 images showing a spot undergoing Ω-enlarge-stay (yellow arrow heads) at -1 s (left), 0 s (middle left, spot onset), 2 s (middle right), and 20 s (right) after the spot onset (time 0). The spot enlargement is not due to focal plane changes, because a pre-existing spot in the neighbour (green arrow heads) did not change in size over time. The pre-existing spot may be due to a stay fusion before stimulation.

(b) STED images showing a spot undergoing Ω-shrink-stay (yellow arrow heads) at -1 s (left), 0 s (middle left), 1 s (middle right), and 4 s (right) after the spot onset (time 0). This spot is the same as the one shown in Fig. 5b. The spot shrinkage is not due to focal plane changes, because a pre-existing fluorescent structure in the neighbour (green arrow heads) did not change in size over time. The pre-existing fluorescent structure may be due to the membrane curvature or a stay fusion occurring before stimulation.

(c) STED images showing a spot undergoing Ω-shrink (yellow arrow heads) at -1 s, 0 s (spot onset), 0.078 s, 0.26 s, and 0.52 s after the spot onset (time 0). This spot is the same as the one shown in Fig. 6c. The spot shrinkage is not due to focal plane changes, because a pre-existing fluorescent spot in the neighbour (green arrow heads) did not change in size over time. The pre-existing fluorescent spot may be due to a stay fusion occurring before stimulation or a membrane curvature.

Conclusion: the spot size change is not due to general focal plane changes, such as the movement of the objective and the stage.

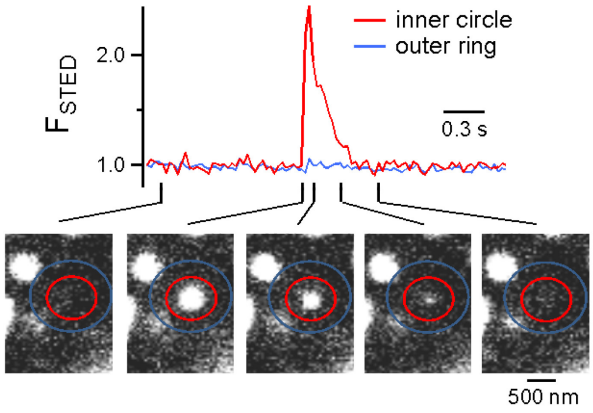

Figure S6. No membrane movement surrounding the spot while the spot is changing size

Re-plot of Figure S5c at a different intensity scale so that the background can be better observed (lower). The fluorescence intensity (F_{STED}) within the spot (inner circle, red) and surrounding the spot (blue, the ring between red and blue circles) are also plotted as a function of time (upper). The images were taken at times indicated by lines.

Conclusion: When the spot was shrinking, F_{STED} was reduced within the spot (inner circle), but did not change immediately outside the spot (outer ring), suggesting that the membrane area immediately surrounding the spot does not move towards the cytosol. This conclusion is based on the logic that a local membrane movement towards the cytosol would increase the distance and thus the fluorescence solution between the membrane and the coverslip, which would increase the fluorescence intensity.

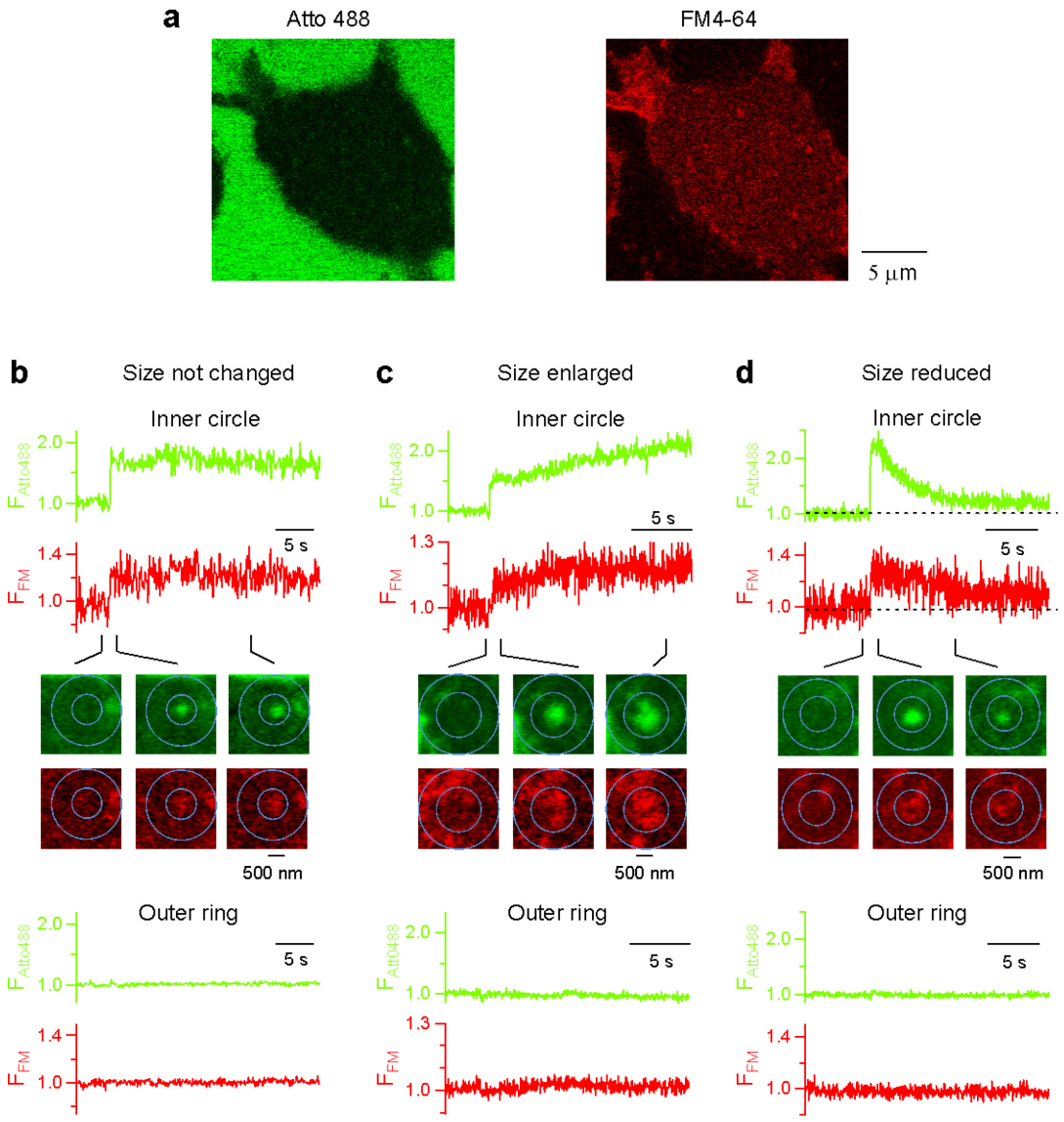

Figure S7. Imaging with Atto 488 and FM4-64 in the bath

(**a**) A cell imaged with Atto 488 (left) and FM4-64 (right) in the bath at the confocal cell-bottom setting. The cell foot print is dark for the Atto 655 image, indicating the depth of the bath solution between the coverslip and the cell bottom membrane is much thinner than the height of the solution surrounding the cell. The cell foot print is bright for the FM4-64 image, because FM4-64 is much brighter at the cell membrane than in the solution.

(**b-d**) Fluorescence intensity of Atto 488 ($F_{Atto488}$, green), FM4-64 (F_{FM}, red), and sampled images (average of 10-15, lines indicate times) are plotted versus time for spots that remained unchanged in size (b), enlarged (c) or reduced in size (d), as determined from Atto 488 imaging. $F_{Atto488}$ and F_{FM} within the spot (smaller circle in images; upper two traces) and surrounding the spot (the outer ring in images – the ring between two circles; lower two traces) are plotted. All four traces have the same time scale. These plots show no change of fluorescence surrounding the spot (lower

two traces) while spots changed in size (upper two traces). Images were collected at the confocal cell-bottom setting with Atto 488 (24 μM) and FM4-64 (12 μM) in the bath. Both dyes were excited only weakly to avoid bleaching. Thus, we do not know whether the pore is closed or not in these experiments. The stimulation was 1 s depolarization.

Note that some large FM4-64 spots' center (granule center) was dimmer (e.g., panels c and d), because FM4-64 at the vesicular membrane is much brighter than in the granule lumen. FM4-64 spots were somewhat like VAMP2-EGFP spots (Fig. 10), which also label vesicular membrane.

Conclusion: These results show no local membrane movement surrounding the spot (outer ring) while the spot (inner circle) may change in size.

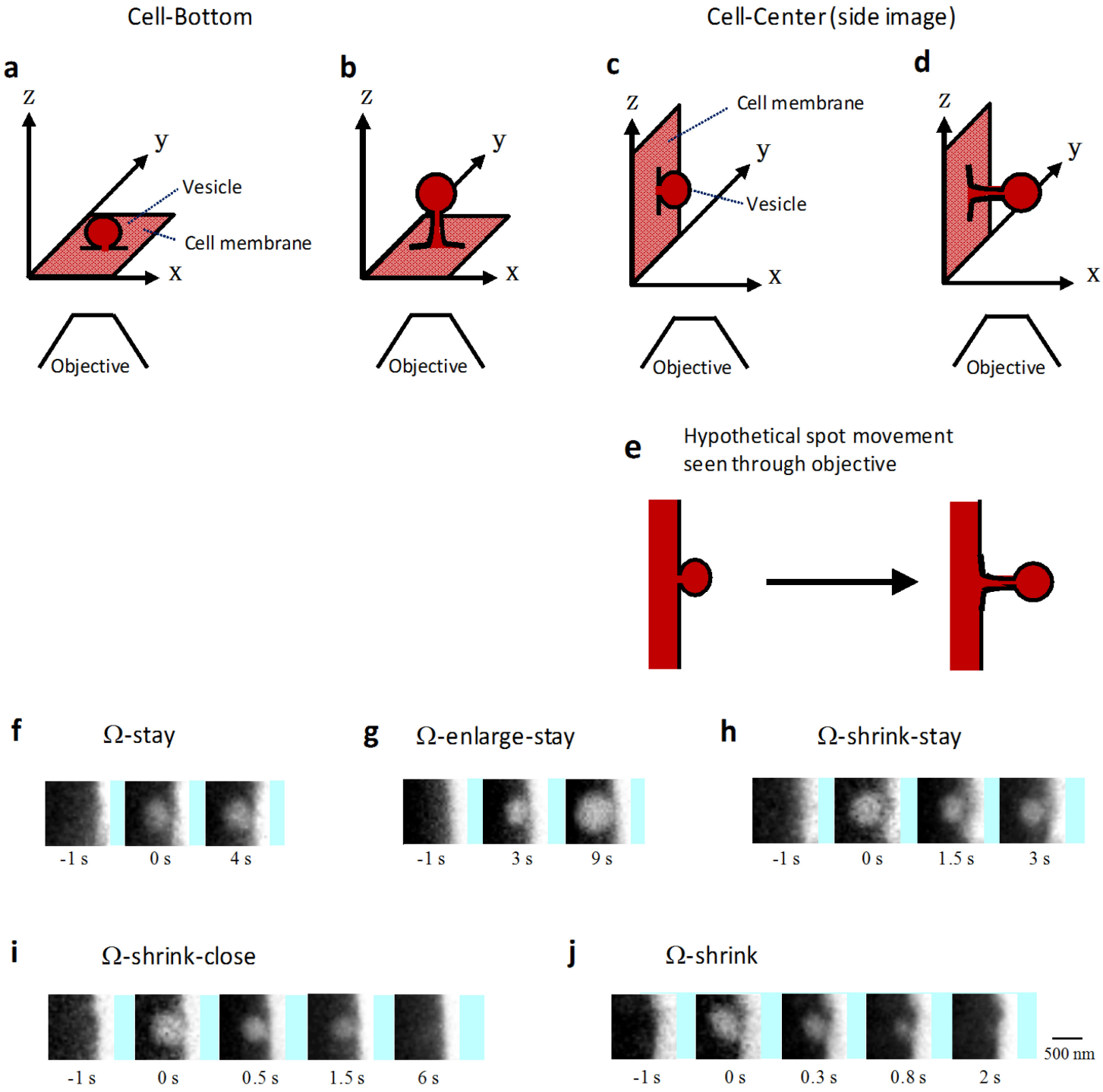

Figure S8. No spot movement perpendicular to the plasma membrane

(**a**) A schematic drawing of a Ω-profile at the cell-bottom image setting, at which the cell-bottom membrane is parallel to the microscopic x/y plane.

(**b**) Similar to panel a, except that the Ω-profile is pushed into the cytosol at a direction perpendicular to the plasma membrane (the microscopic z direction).

(**c**) A schematic drawing of a Ω-profile at the cell-center setting, at which the plasma membrane is parallel to the microscopic z axis.

(**d**) Similar to panel c, except that the Ω-profile is pushed into the cytosol (perpendicular to the plasma membrane) by membrane movement in the microscopic x axis.

(**e**) Hypothetical movement of the Ω-profile from panel c to d as seen through the objective (top-down view). Red color indicates fluorescent dye at the extracellular side.

(**f-j**) Experimental results collected at the STED cell-center setting indicating no hypothetical movement illustrated in panel e. Note: for the convenience of drawing, the extracellular side is positioned in the left side in panels c-e. In contrast, the extracellular side is positioned in the right side for experimental STED cell-center images in panels f-j, because we always show images at the cell-center setting in this way. The time labeled in images refers to the time relative to the spot onset (onset time is set as 0).

f, Ω-stay (same as Fig. 3c); **g,** Ω-enlarge-stay (same as Fig. 4b); **h,** Ω-shrink-stay (same as Fig. 5c); **i,** Ω-shrink-close (same as Fig. 5f); **j,** Ω-shrink (same as Fig. 6d). The scale bar in panel j applies to panels f-j.

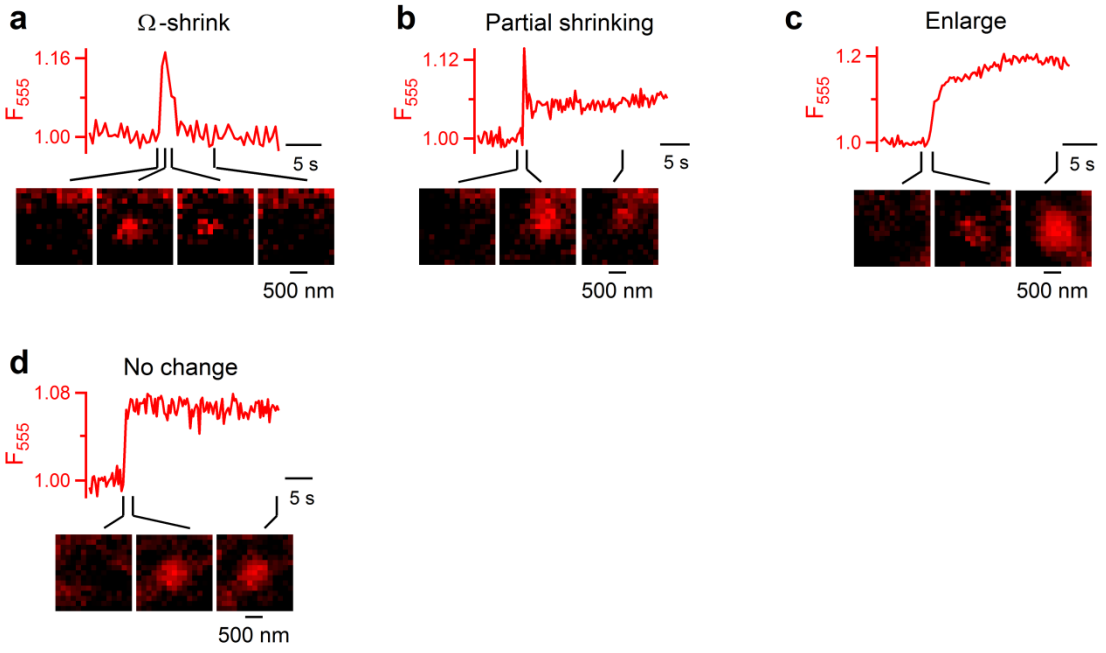

Figure S9. The spot size may shrink, enlarge or remain unchanged in TIRF imaging (**a-d**) TIRF imaging shows that the Alexa 555 spots induced by $depol_{1s}$ may shrink completely (a, Ω-shrink), shrink partially (b), enlarge (c), or remain unchanged (d). The fluorescence intensity of Alexa 555 spots (F_{555}) is shown in the upper panel. The representative images taken at times indicated by the lines are shown in the lower panel. The bath contained 30 μM Alexa 555. Since TIRF imaging could not rapidly bleach the whole vesicle after pore closure, it is difficult to distinguish whether the Ω-$profile_{fusion}$'s pore is close or open. Thus, partial shrinking may mean Ω-shrink-stay or Ω-shrink-close; enlarge may mean Ω-enlarge-stay or Ω-enlarge-close; and no change may refer to Ω-stay or Ω-close.

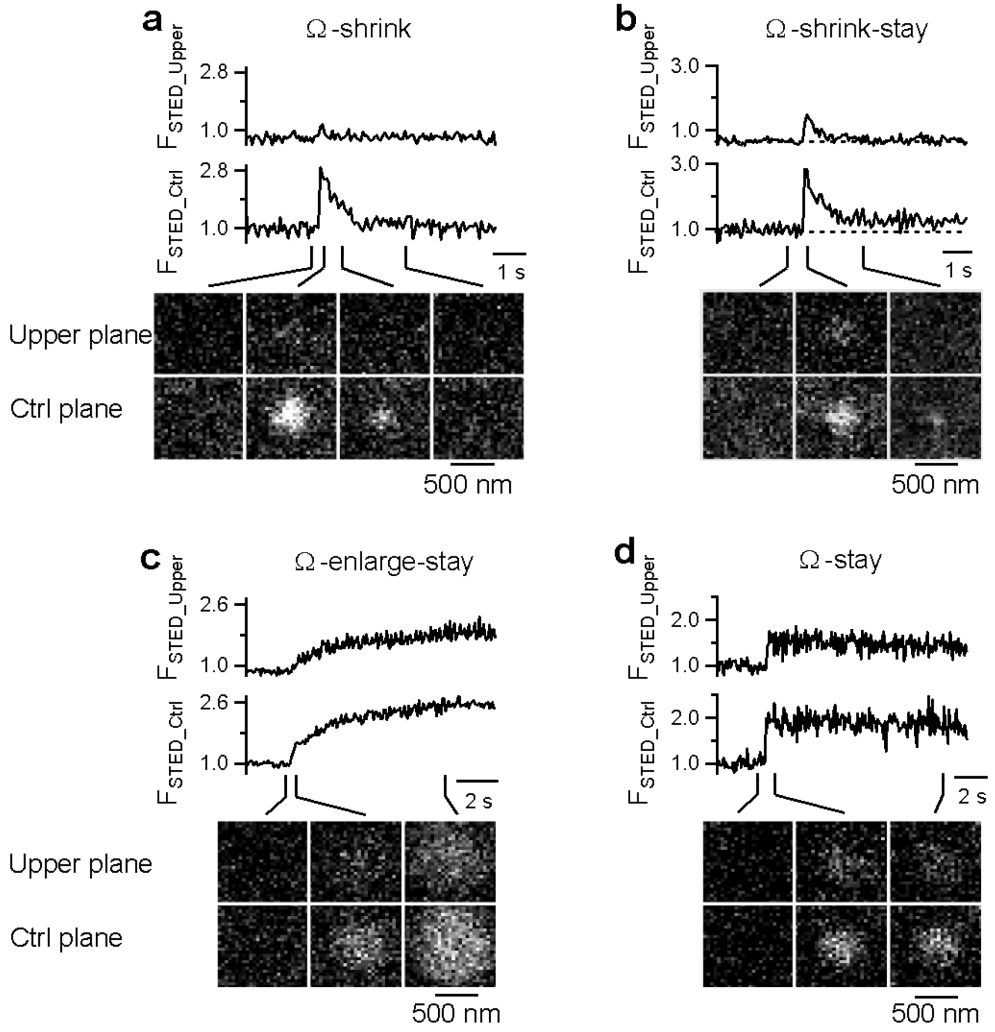

Figure S10. STED imaging at two focal planes shows no spot movement along the microscopic z axis

(a) Ω-shrink: F_{STED} of a spot (induced by $depol_{1s}$) imaged at the cell-bottom control focal plane (F_{STED_Ctrl}, lower) and a focal plane 300 nm above (F_{STED_Upper}, upper) at the STED cell-bottom setting. Sampled images (average of 5) at times indicated (lines) from the control (lower) and the upper focal plane (upper) are also shown. F_{STED} at both focal planes was normalized to the mean value before the spot appeared at the control focal plane (applies to all plots in this figure). The focal plane was switched every 70 ms to collect images at both focal planes.

(b-d) Similar to panel a, but for spots undergoing Ω-shrink-stay (b), Ω-enlarge-stay (c), and Ω-stay (d).

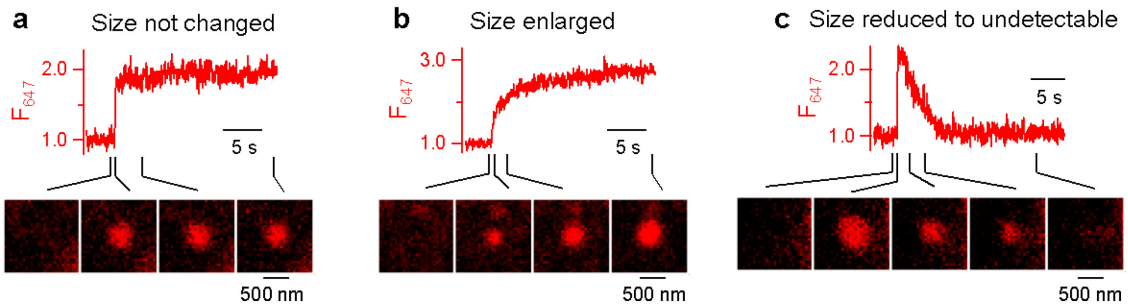

Figure S11. The spot size change observed under weak excitation

(**a**) F_{647} and sampled images (average of 5) at times indicated (lines) are plotted versus time for a spot undergoing no change of the size at the confocal microscope with A647 in the bath. A647 was excited weakly so that the bleaching was insignificant even when the pore was closed. F_{647} was normalized to the mean value before spot appeared. Spots were induced by $depol_{1s}$ and images were collected every 45 ms.

(**b-c**) Similar to panel a, except for spots undergoing enlargement (b) or shrinkage (c). The spot in panel c shrank until undetectable, reflecting Ω-shrink fusion.

Conclusion: Spot size change is observed with weak excitation, indicating that the spot size change is not due to photo-toxicity caused by strong excitation.

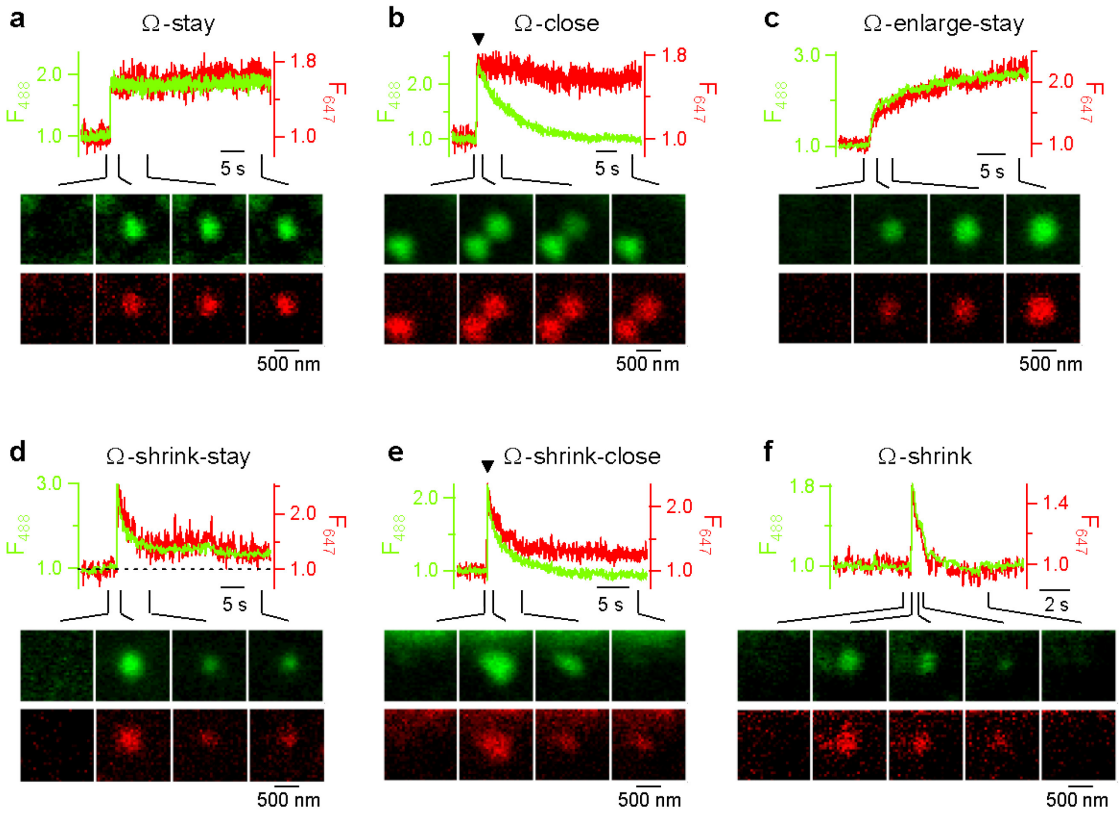

Figure S12. Examples of various fusion modes observed at confocal cell-bottom A488 (strong excitation)/A647 (weak excitation) setting

(**a-f**) F_{488} (green), F_{647} (red), and sampled images (average of 5) at times indicated (lines) are plotted versus time for spots undergoing Ω-stay (a), Ω-close (b), Ω-enlarge-stay (c), Ω-shrink-stay (d), Ω-shrink-close (e), and Ω-shrink (f). The spots were imaged under the confocal microscope with A488 and A647 in the bath, but with strong excitation for A488 and weak excitation for A647. F_{488} and F_{647} were normalized to the mean value before spot appeared. Spots were induced by $depol_{1s}$ and images were collected every 45 ms. In panel b, a pre-existing spot (left lower corner) indicates no change of the focal plane.

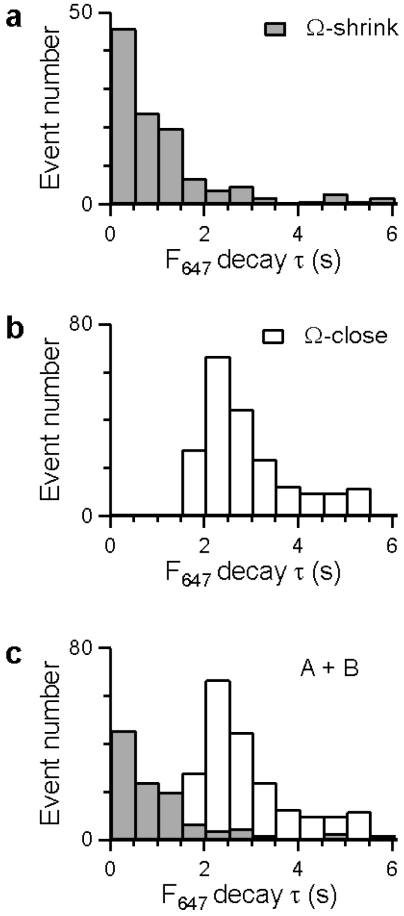

Figure S13. Time constant of F_{647} decay during Ω-shrink and Ω-close fusion

(**a**) The number of events is plotted versus the time constant (τ) of the F_{647} decay during Ω-shrink fusion (solid). The data were obtained from confocal/cell-bottom/A647/A488 experiments and binned every 0.5 s (applies to panel a-c).

(**b**) The number of events is plotted versus the F_{647} decay τ during Ω-close (open) fusion.

(**c**) The number of events for Ω-shrink (solid bar) and Ω-close (open) plotted versus the F_{647} decay τ. This plot is simply an addition of pane b on top of panel a, allowing for easier comparison of panels a and b.

Conclusion: 1) when F_{647} decay time constant is less than 1.7 s (binned every 0.5 and thus was seen as less than 1.5 s in panel C), all events are Ω-shrink fusion; and 2) when F_{647} decay time constant is more than 2 s, 92% of events are Ω-close fusion (panel c).